Progress In Electromagnetics Research M, Vol. 43, 135–145, 2015

Electromagnetic Characteristics of 1D Grapheme Photonic Crystal by Using SBC-FDTD Method of Oblique Incidence in THz

Lixia Yang[1, *], Lingling Li[1], and Lunjin Chen[2]

Abstract—A modified 1D finite-difference time-domain method is analyzed by using the surface boundary condition (SBC-FDTD) for oblique incidence. The SBC-FDTD iterative formulas are deduced in oblique incidence by TE_z and TM_z wave. The reflection and transmission coefficients of electromagnetic wave in the 1D photonic crystal (PC) including a graphene sheet are calculated by the SBC-FDTD method. The method is also validated by comparison with the existed analytic methods. Finally, this modified method is applied to simulate 1D graphene photonic crystal (GPC). By changing the position of grapheme sheet in GPC, the electromagnetic gap characterizations of 1D GPC by an oblique incidence plane wave in THz spectral range are studied. The computational results show that the graphene sheet can enhance the absorption in THz because of the localization of light and the surface defect formed by graphene.

1. INTRODUCTION

Graphene consists of a single layer of carbon atoms, which is organized in a hexagonal honey-comb structure. It has been known for good conductivity, zero band gap structure and unique light sensitive features [1, 2]. As a novel two-dimensional semi-conductor material, the graphene has drawn a great deal of interest since successful stripping in 2004 [3].

Recently, the studies tend to focus on the electromagnetic characterizations of graphene in THz spectral range and the attempt of adding graphene into various opto-electronic devices. One of the common goals is to enhance the power absorption of graphene in THz [4]. In 2012, Liu et al. studied the power absorption of graphene by adding graphene on the top of one-dimensional photonic crystal. The results show the absorption efficiency of this kind of structure is superior to that of monolayer graphene [5]. In 2013, Nayyeri et al. proposed a modeling for graphene by the FDTD method using a surface boundary condition (SBC), but the study is limited to parallel incidence [6]. In this paper, we extend the SBC for oblique incidence and propose a FDTD method that can transform two-dimensional scattering problem of electromagnetic wave to one-dimensional condition [7]. By using the modified SBC-FDTD method, the reflection and transmission coefficients of electromagnetic wave in the 1D GPC with a graphene sheet located at various position are calculated in THz. The results show that the absorption performance is optimized when the graphene is located on the top of the photonic crystal.

2. PARAMETERS OF GRAPHENE

A scalar surface conductivity of graphene can be represented symbolically as $\sigma_g(\omega, \mu_c, \Gamma, T)$, depending on frequency ω, chemical potential μ_c (which can be controlled by either an applied electrostatic bias or doping), phenomenological scattering rate Γ, and temperature T [8]. The conductivity of

Received 29 June 2015, Accepted 9 August 2015, Scheduled 27 August 2015

* Corresponding author: Lixia Yang (lixiayang@yeah.net).

[1] Department of Communication Engineering, Jiangsu University, Zhenjiang 212000, China. [2] Department of Physics, University of Texas at Dallas, Richardson 75355, USA.

graphene has been commonly expressed by the well-known Kubo formula consisting of two terms, $\sigma_g = \sigma_{\text{intra}} + \sigma_{\text{inter}}$, where the former is due to the intraband contributions and the latter is due to the interband contributions. In general, the interband term is negligible and the intraband term is dominant [8]. σ_{intra} can be evaluated by Drude-like expression as

$$\sigma_{\text{intra}}(\omega, \mu_c, \Gamma, T) = \frac{\sigma_0}{1 + j\omega\tau} \tag{1}$$

where

$$\sigma_0 = \frac{e^2 \tau k_B T}{\pi \hbar^2} \left[\frac{\mu_c}{k_B T} + 2Ln\left(\exp\left\{-\mu_c / k_B T\right\} + 1\right) \right]$$

is the dc conductivity, e the electron charge, k_B the Boltzmann constant, $\hbar$ the reduced Planck constant, and $\tau = 1/(2\Gamma)$ the phenomenological electron relaxation time. Eq. (1) is adopted as the surface conductivity model of a graphene sheet in our study.

2.1. Oblique Incidence by TE$_z$ Wave

Firstly, we consider a one-dimensional problem where a TE$_z$ polarized plane wave is obliquely incident on a conducting sheet at an angle θ. The 1-D FDTD mesh including a graphene sheet at the spatial grid $K + 1/2$ is shown in Fig. 1, where the tangential component E_y of electric field and the tangential component H_x of magnetic field are staggered at one-half cell. H_z is the normal component of magnetic field. Since a conductive material allows for the possibility of conduction current, we consider two magnetic fields, ${}^1H_x$ and ${}^2H_x$ immediately to the left and right sides of the conductive sheet boundary [6].

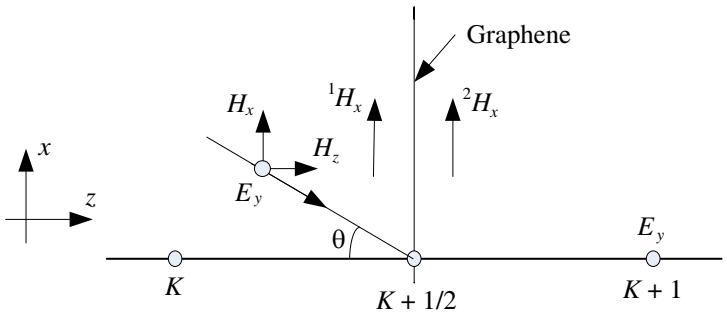

Figure 1. TE$_z$ polarized plane wave with oblique incident.

According to Maxwell's curl equations [9], the time domain Maxwell's equations of TE$_z$ polarized plane wave in vacuum are

$$\begin{cases} \dfrac{\partial H_x}{\partial z} - \dfrac{\partial H_z}{\partial x} = \varepsilon_0 \dfrac{\partial E_y}{\partial t} \\ \dfrac{\partial E_y}{\partial z} = \mu_0 \dfrac{\partial H_x}{\partial t} \\ \dfrac{\partial E_y}{\partial x} = -\mu_0 \dfrac{\partial H_z}{\partial t} \end{cases} \tag{2}$$

By converting Eq. (2) from time domain to frequency domain of via Fourier transform, we have

$$\begin{cases} \dfrac{\partial H_x}{\partial z} - \dfrac{\partial H_z}{\partial x} = j\omega\varepsilon_0 E_y \\ \dfrac{\partial E_y}{\partial z} = j\omega\mu_0 H_x \\ \dfrac{\partial E_y}{\partial x} = -j\omega\mu_0 H_z \end{cases} \tag{3}$$

Then, the one-dimensional solution of electromagnetic waves along x direction is

$$\begin{cases} E_{y1\text{D}} = E_0 e^{jk\sin\theta x + j\omega t} \\ H_{z1\text{D}} = -\sin\theta \dfrac{E_0}{\eta_0} e^{jk\sin\theta x + j\omega t} \end{cases} \tag{4}$$

By substituting Eq. (4) into Eq. (3) for eliminating H_z and then converting the expressions from frequency domain to time domain via $j\omega \to \partial/\partial t$, we have

$$\begin{cases} \dfrac{\partial E_{y1\mathrm{D}}}{\partial z} = \mu_0 \dfrac{\partial H_{x1\mathrm{D}}}{\partial t} \\ \dfrac{1}{\cos^2\theta}\dfrac{\partial H_{x1\mathrm{D}}}{\partial z} = \varepsilon_0 \dfrac{\partial E_{y1\mathrm{D}}}{\partial t} \end{cases} \tag{5}$$

Therefore, FDTD iterative formulas of one-dimensional Maxwell's equations for vacuum are

$$\begin{cases} E_y^{n+1}(k) = E_y^n(k) + \dfrac{\Delta t}{\varepsilon_0 \cos^2\theta \Delta z}\left[H_x^{n+1/2}(k+1/2) - H_x^{n+1/2}(k-1/2)\right] \\ H_x^{n+1/2}(k+1/2) = H_x^{n-1/2}(k+1/2) + \dfrac{\Delta t}{\mu_0 \Delta z}\left[E_y^n(k+1) - E_y^n(k)\right] \end{cases} \tag{6}$$

When there is a graphene sheet, we discretize Faraday's law $\partial \mathbf{B}/\partial t = -\nabla \times \mathbf{E}$ at the grid $K+1/2$ such that the central difference scheme is used for the time derivative $\partial \mathbf{B}/\partial t$, and backward and forward difference schemes are used for spatial derivative along the z direction:

$$\begin{cases} \mu_1 \delta_t^c \left\{{}^1H_x^n\right\} = \delta_z^b \left\{E_y^n(K+1/2)\right\} \\ \mu_2 \delta_t^c \left\{{}^2H_x^n\right\} = \delta_z^f \left\{E_y^n(K+1/2)\right\} \end{cases} \tag{7}$$

where μ_1 and μ_2 are the permeabilities of media to the left and right sides of the interface respectively, and δ^c, δ^b and δ^f are the central, backward and forward difference derivative approximations, we have

$$\begin{cases} \mu_1 \dfrac{{}^1H_x^{n+1/2}(K+1/2) - {}^1H_x^{n-1/2}(K+1/2)}{\Delta t} = \dfrac{E_y^n(K+1/2) - E_y^n(K)}{\Delta z/2} \\ \mu_2 \dfrac{{}^2H_x^{n+1/2}(K+1/2) - {}^2H_x^{n-1/2}(K+1/2)}{\Delta t} = \dfrac{E_y^n(K+1) - E_y^n(K+1/2)}{\Delta z/2} \end{cases} \tag{8}$$

Using the boundary condition at the conducting surface [6],

$${}^2H_x(K+1/2) - {}^1H_x(K+1/2) = \sigma_g E_y(K+1/2) \tag{9}$$

By substituting $E_y(K+1/2)$ into Eq. (8), we obtain

$$\begin{cases} \dfrac{\mu_1}{\Delta t}\left[{}^1H_x^{n+1/2}(K+1/2) - {}^1H_x^{n-1/2}(K+1/2)\right] \\ = \dfrac{2}{\Delta z}\left\{\dfrac{1+j\omega t}{\sigma_0}\left[{}^2H_x^n(K+1/2) - {}^1H_x^n(K+1/2)\right] - E_y^n(K)\right\} \\ \dfrac{\mu_2}{\Delta t}\left[{}^2H_x^{n+1/2}(K+1/2) - {}^2H_x^{n-1/2}(K+1/2)\right] \\ = \dfrac{2}{\Delta z}\left\{E_y^n(K+1) - \dfrac{1+j\omega t}{\sigma_0}\left[{}^2H_x^n(K+1/2) - {}^1H_x^n(K+1/2)\right]\right\} \end{cases} \tag{10}$$

Converting the expressions from frequency domain to time domain via $j\omega \to \partial/\partial t$, we have

$$\begin{aligned} & \frac{\mu_1}{\Delta t}\left[{}^1H_x^{n+1/2}(K+1/2) - {}^1H_x^{n-1/2}(K+1/2)\right] \\ = \; & \frac{2}{\Delta z \sigma_0}\left[{}^2H_x^n(K+1/2) - {}^1H_x^n(K+1/2)\right] \\ & + \frac{2t}{\Delta z \sigma_0}\frac{\partial}{\partial t}\left[{}^2H_x^n(K+1/2) - {}^1H_x^n(K+1/2)\right] - \frac{2}{\Delta z}E_y^n(K) \end{aligned} \tag{11}$$

$$\begin{aligned} & \frac{\mu_2}{\Delta t}\left[{}^2H_x^{n+1/2}(K+1/2) - {}^2H_x^{n-1/2}(K+1/2)\right] \\ = \; & \frac{2}{\Delta z}E_y^n(K+1) - \frac{2}{\Delta z \sigma_0}\left[{}^2H_x^n(K+1/2) - {}^1H_x^n(K+1/2)\right] \\ & - \frac{2t}{\Delta z \sigma_0}\frac{\partial}{\partial t}\left[{}^2H_x^n(K+1/2) - {}^1H_x^n(K+1/2)\right] \end{aligned} \tag{12}$$

where the values of the magnetic field components at time step n are approximated by the average of the field values at $n-1/2$ and $n+1/2$

$$H_x^n\left(K+1/2\right)=\frac{H_x^{n+1/2}\left(K+1/2\right)+H_x^{n-1/2}\left(K+1/2\right)}{2} \tag{13}$$

By substituting Eq. (13) into Eqs. (11) and (12), the updating equations for ${}^1H_x$ and ${}^2H_x$ can be obtained

$$\begin{aligned}
{}^1H_x^{n+1/2}\left(K+1/2\right) &= \frac{1}{1-c_1c_2}\Big\{\left(f_{h11}+c_1f_{h21}\right){}^1H_x^{n-1/2}\left(K+1/2\right) && (14)\\
&\quad +\left(f_{h12}+c_1f_{h22}\right){}^2H_x^{n-1/2}\left(K+1/2\right)+2c_1f_{e2}E_y^n\left(K+1\right)-2f_{e1}E_y^n(K)\Big\} && (15)\\
{}^2H_x^{n+1/2}\left(K+1/2\right) &= \frac{1}{1-c_1c_2}\Big\{\left(f_{h21}+c_2f_{h11}\right){}^1H_x^{n-1/2}\left(K+1/2\right) && (16)\\
&\quad +\left(f_{h22}+c_2f_{h12}\right){}^2H_x^{n-1/2}\left(K+1/2\right)+2f_{e2}E_y^n\left(K+1\right)-2c_2f_{e1}E_y^n(K)\Big\} && (17)
\end{aligned}$$

where $c_1=\frac{\Delta t+2t}{\mu_1\Delta z\sigma_0+\Delta t+2t}$; $c_2=\frac{\Delta t+2t}{\mu_2\Delta z\sigma_0+\Delta t+2t}$; $f_{e1}=\frac{\Delta t\sigma_0}{\mu_1\Delta z\sigma_0+\Delta t+2t}$; $f_{e2}=\frac{\Delta t\sigma_0}{\mu_2\Delta z\sigma_0+\Delta t+2t}$; $f_{h11}=1-\frac{2\Delta t}{\mu_1\Delta z\sigma_0+\Delta t+2t}$; $f_{h12}=\frac{\Delta t-2t}{\mu_1\Delta z\sigma_0+\Delta t+2t}$; $f_{h21}=\frac{\Delta t-2t}{\mu_2\Delta z\sigma_0+\Delta t+2t}$; $f_{h22}=1-\frac{2\Delta t}{\mu_2\Delta z\sigma_0+\Delta t+2t}$.

2.2. Oblique Incidence by TM$_z$ Wave

Similarly, we consider the one-dimensional problem that a TM$_z$ polarized plane wave is obliquely incident on a conducting sheet at an angle θ. The 1-D FDTD mesh including a graphene sheet at the spatial grid $K+1/2$ is shown in Fig. 2, where the tangential component E_x of the electric field and the tangential component H_y of the magnetic field are staggered at one-half cell apart. E_z is the normal component of the electric field. Similar to oblique incidence situation of TE$_z$ wave in Section 1.1, we consider two magnetic fields, ${}^1H_y$ and ${}^2H_y$ immediately to the left and right sides of the conductive sheet boundary [6].

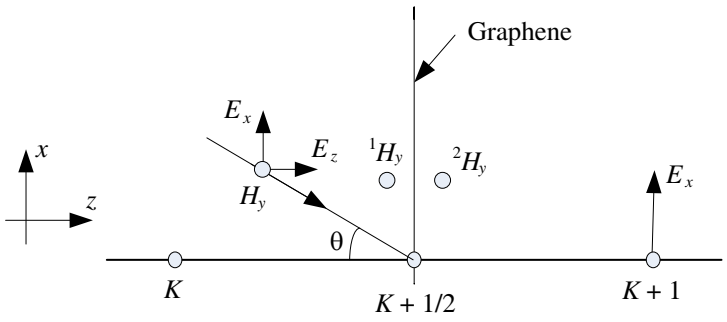

Figure 2. TM$_z$ polarized plane wave oblique incident.

According to Maxwell's curl equations, the time domain Maxwell's equations of TM$_z$ polarized plane wave about vacuum are

$$\begin{cases}
\dfrac{\partial E_x}{\partial z}-\dfrac{\partial E_z}{\partial x}=-\mu_0\dfrac{\partial H_y}{\partial t}\\
-\dfrac{\partial H_y}{\partial z}=\varepsilon_0\dfrac{\partial E_x}{\partial t}\\
\dfrac{\partial H_y}{\partial x}=\varepsilon_0\dfrac{\partial E_z}{\partial t}
\end{cases} \tag{18}$$

The same to TE$_z$ case, FDTD iterative formulas of one-dimensional Maxwell's equations of TM$_z$

polarized plane wave for vacuum are

$$\begin{cases} E_x^{n+1}(k) = E_x^n(k) - \dfrac{\Delta t}{\varepsilon_0 \Delta z}\left[H_y^{n+1/2}(k+1/2) - H_y^{n+1/2}(k-1/2)\right] \\ H_y^{n+1/2}(k+1/2) = H_y^{n-1/2}(k+1/2) - \dfrac{\Delta t}{\mu_0 \cos^2\theta \Delta z}\left[E_x^n(k+1) - E_x^n(k)\right] \end{cases} \tag{19}$$

When there is a Graphene sheet, the central difference scheme is used for ${}^1H_y$ and ${}^2H_y$, and backward and forward difference schemes are used for E_x along the z direction:

$$\begin{cases} -\mu_1 \delta_t^c \left\{{}^1H_y^n\right\} = \dfrac{1}{\cos^2\theta} \cdot \delta_z^b \left\{E_x^n(K+1/2)\right\} \\ -\mu_2 \delta_t^c \left\{{}^2H_y^n\right\} = \dfrac{1}{\cos^2\theta} \cdot \delta_z^f \left\{E_x^n(K+1/2)\right\} \end{cases} \tag{20}$$

where μ_1 and μ_2 are the permeabilities of media at the left and right sides of the interface, and δ^c, δ^b and δ^f are the central, backward and forward difference derivative approximations.

Using the boundary condition at the conducting surface [10],

$${}^2H_y(K+1/2) - {}^1H_y(K+1/2) = -\sigma_g E_x(K+1/2) \tag{21}$$

The derivation process is similar to TE_z, and we will repeat no more. The updating equations for ${}^1H_y$ and ${}^2H_y$ can be obtained

$$\begin{aligned} {}^1H_y^{n+1/2}(K+1/2) &= \frac{1}{1-c_1c_2}\Big\{(f_{h11} + c_1 f_{h21})\,{}^1H_y^{n-1/2}(K+1/2) && (22) \\ &\quad + (f_{h12} + c_1 f_{h22})\,{}^2H_y^{n-1/2}(K+1/2) - 2c_1 f_{e2} E_x^n(K+1) + 2f_{e1}E_x^n(K)\Big\} && (23) \\ {}^2H_y^{n+1/2}(K+1/2) &= \frac{1}{1-c_1c_2}\Big\{(f_{h21} + c_2 f_{h11})\,{}^1H_y^{n-1/2}(K+1/2) && (24) \\ &\quad + (f_{h22} + c_2 f_{h12})\,{}^2H_y^{n-1/2}(K+1/2) - 2f_{e2} E_x^n(K+1) + 2c_2 f_{e1}E_x^n(K)\Big\} && (25) \end{aligned}$$

where $c_1 = \frac{\Delta t+2t}{\mu_1 \Delta z \sigma_0 \cos^2\theta + \Delta t + 2t}$; $c_2 = \frac{\Delta t+2t}{\mu_2 \Delta z \sigma_0 \cos^2\theta + \Delta t + 2t}$; $f_{e1} = \frac{\Delta t \sigma_0}{\mu_1 \Delta z \sigma_0 \cos^2\theta + \Delta t + 2t}$; $f_{e2} = \frac{\Delta t \sigma_0}{\mu_2 \Delta z \sigma_0 \cos^2\theta + \Delta t + 2t}$; $f_{h11} = 1 - \frac{2\Delta t}{\mu_1 \Delta z \sigma_0 \cos^2\theta + \Delta t + 2t}$; $f_{h12} = \frac{\Delta t - 2t}{\mu_1 \Delta z \sigma_0 \cos^2\theta + \Delta t + 2t}$; $f_{h21} = \frac{\Delta t - 2t}{\mu_2 \Delta z \sigma_0 \cos^2\theta + \Delta t + 2t}$; $f_{h22} = 1 - \frac{2\Delta t}{\mu_2 \Delta z \sigma_0 \cos^2\theta + \Delta t + 2t}$.

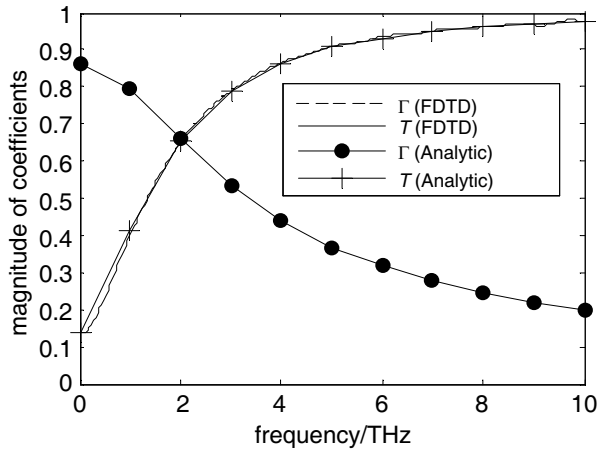

Figure 3. The transmission and reflection coefficients for TE_Z with incidence angle $\theta = 30°$.

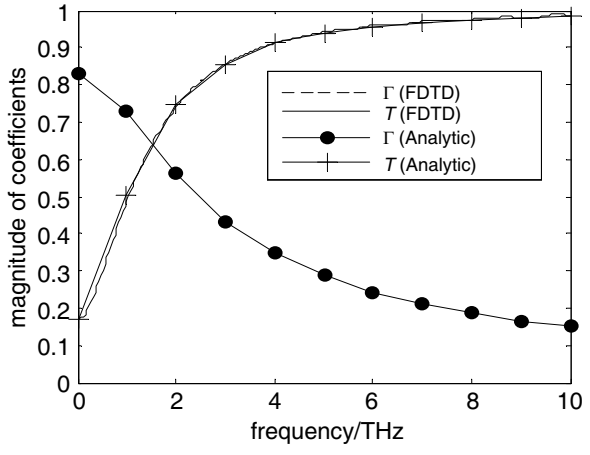

Figure 4. The transmission and reflection coefficients for TM_Z with incidence angle $\theta = 30°$.

2.3. Numerical Validation

For verifying the accuracy of the algorithm, we calculate the reflection and transmission coefficients when plane wave is obliquely incident on a graphene sheet with angle θ by using the above algorithm. A Gaussian pulse $E_i(t) = \exp(-\frac{4\pi(t-t_0)^2}{\tau_1^2})$ is used as the source which the highest frequency effectively is $f_{\max} = 10\,\text{THz}$, $t_0 = 1.6 \times 10^{13}\,\text{s}$, $\tau_1 = 2/f_{\max}$. The FDTD spatial mesh is set to $\Delta z = 1.5 \times 10^{-6}\,\text{m}$, and the time step is set to $\Delta t = \Delta z/c/2 = 2.5 \times 10^{-15}\,\text{s}$. The speed of light is $c = 3 \times 10^8\,\text{m/s}$. The simulation was run for 10000 time steps. We consider a graphene sheet of $T = 300\,\text{K}$, $\mu_c = 0.5\,\text{eV}$, $\tau = 0.5\,\text{ps}$, $\varepsilon = 1.0$.

The transmission and reflection coefficients are also calculated analytically as $T = 2\cos\theta/(2\cos\theta + \eta_0\sigma_0)$ and $\Gamma = T - 1$ for TE_Z [11], where η_0 is the free space impedance. Fig. 3 shows the comparison with numerical examples of $\theta = 30°$.

The transmission and reflection coefficients are calculated analytically as $T = 2/(2 + \eta_0\sigma_0\cos\theta)$ and $\Gamma = T - 1$ for TM_Z [11], where η_0 is the free space impedance. Fig. 4 shows the comparison with numerical examples of $\theta = 30°$.

From Fig. 3 and Fig. 4, the transmission and reflection coefficients calculated by the SBC-FDTD method are identical with the analytic solutions. The results show that the method is feasible. The absorption performance of the monolayer graphene is great in the high frequency of THz, where the transmission coefficient is above 0.98 even close to 1, while the reflection coefficients is nearly 0.15.

3. 1D GPC BY OBLIQUE INCIDENCE

Increasing researches focus on the characters of the optical absorption enhancement for graphene in THz, which provides a theoretical foundation for the investigation of GPC and its application. In the following sections, three structures about the combinations of graphene and one-dimensional photonic crystal will be simulated by the above-mentioned SBC-FDTD method, respectively. In the simulations, the polarized plane wave is incident obliquely on three one-dimensional GPCs with θ. A Gaussian pulse is used as the source, which is the same as the validation example.

3.1. Graphene on the Surface of One-Dimensional GPC

In this condition, the Graphene is located on the surface of a structure of a spatially periodic array of Si/SiO_2 which extends for several layers, and the graphene and this structure are separated by a spacer made of SiO_2 (seen in Fig. 5).

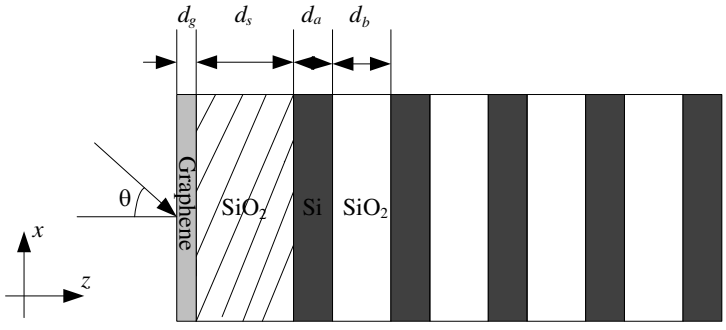

Figure 5. Model of graphene located at surface of the 1D photonic crystal.

In this model, we approximate the dielectric constant of Si by its static value, $\varepsilon_a = 12.96$, and its length is set as $d_a = \lambda_0/4\sqrt{\varepsilon_a}$. Similarly, the dielectric constant of SiO_2 is $\varepsilon_b = 3.64$, with length $d_b = \lambda_0/4\sqrt{\varepsilon_b}$. ε_s, the dielectric constant of the spacer $\varepsilon_s = \varepsilon_b$, with length set as $d_s = \lambda_0/2\sqrt{\varepsilon_s}$ [6]. The center frequency of the THz wave is taken as $f = 5\,\text{THz}$, with the corresponding center wavelength $\lambda_0 = 60\,\mu\text{m}$ [10].

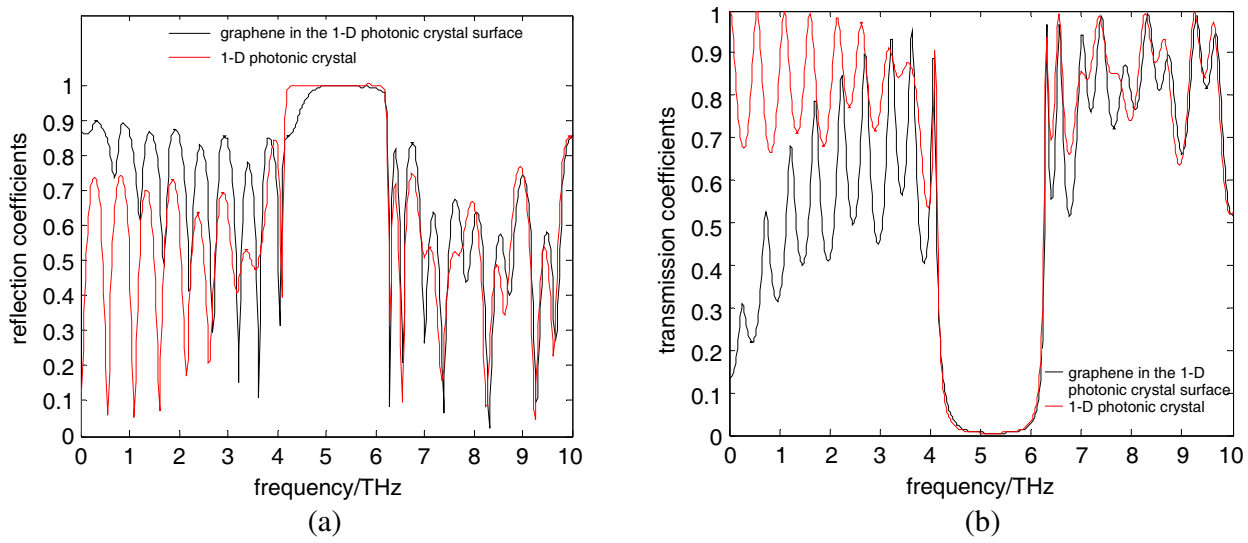

Figure 6. Reflection and transmission coefficients by TE_Z. (a) Reflection coefficients, (b) transmission coefficients.

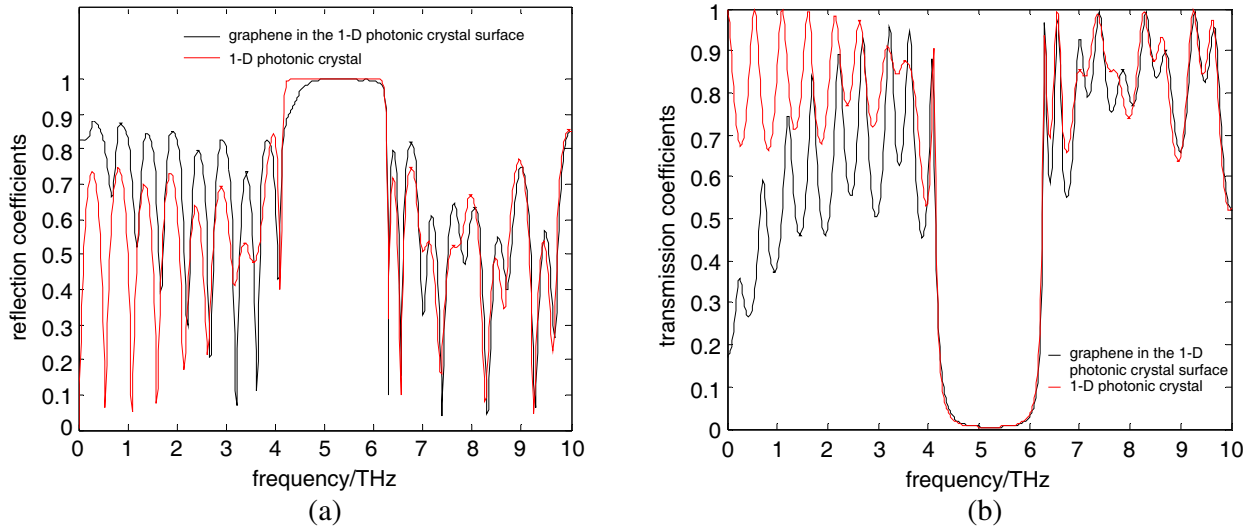

Figure 7. TM_Z Reflection and transmission coefficients by TM_Z. (a) Reflection coefficients, (b) transmission coefficients.

The transmission and reflection coefficients of GPC are given by SBC-FDTD method, with and without graphene respectively, for oblique incidence of TE_Z and TM_Z wave with $\theta = 30°$. The results can be seen in Fig. 6 and Fig. 7. For the reflection coefficient, when the Grapheme is on the surface of GPC the photonic band gap is about 5–6 THz. Compared with the photonic crystal without the grapheme, the photonic band gap is about 4–6 THz. For the transmission coefficient, the location of grapheme almost has nothing effect on the width of the photonic band gap. The reflection coefficient of GPC decreases nearly by 0.25 at 7 THz, and the transmission coefficient increases by 0.2 at 6.8 THz in the TE_Z oblique incidence with $\theta = 30°$, as shown in Fig. 6; the reflection coefficient of GPC decreases, the transmission coefficient also increases in the TM_Z oblique incidence with $\theta = 30°$, which also can be seen in Fig. 7. These results show that the introduction of graphene layer can enhance the absorption power in THz. This is because the surface defect formed by the 1D GPC results in the localization of light, which enhance the transmission of graphene and reduce the reflectivity in THz spectral range [12].

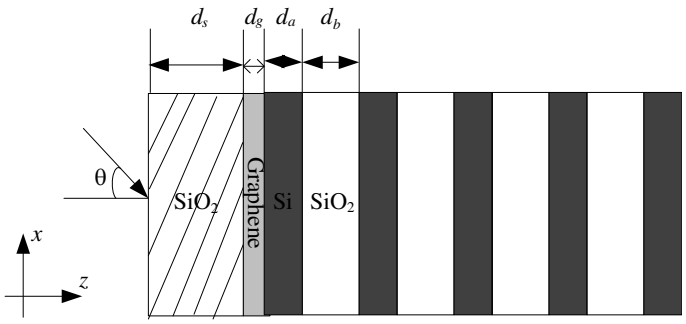

Figure 8. Model of graphene in the middle of 1-D photonic crystal.

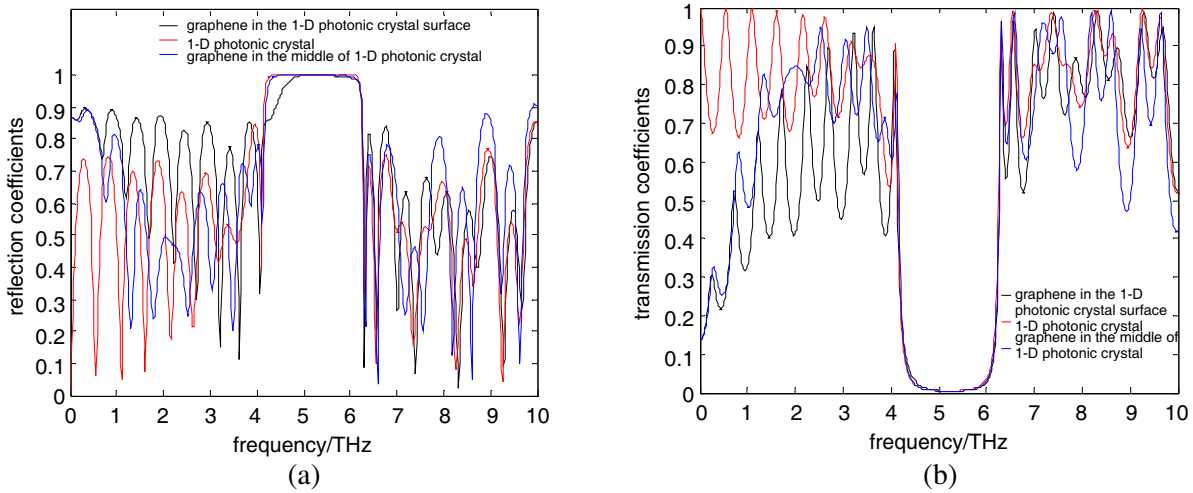

Figure 9. Reflection and transmission coefficients by TE_Z. (a) Reflection coefficients, (b) transmission coefficients.

3.2. Graphene in the Middle of One-Dimensional Graphene Photonic Crystal

The graphene is located between a structure of a spatially periodic array of Si/SiO_2 which extends for several layers and a spacer of SiO_2 (seen in Fig. 8).

The reflection and transmission coefficients of TE_Z and TM_Z wave for oblique incidence with $\theta = 30^\circ$ are shown in Fig. 9 and Fig. 10 by using the SBC-FDTD method. Fig. 9 presents the reflection and transmission coefficients of the TE_Z before and after the graphene is introduced. Fig. 10 shows the same results but for TM_Z. We still present the computed results which can be found as a black line in Fig. 9 and Fig. 10 for the case where the Graphene is added in the middle of 1D PC. The photonic band gap is about 4–6 THz. Compared with the graphene on the surface of 1D PC, we can obtain that the reflection and transmission coefficients are not improved when the graphene is set in the middle of the spacer and 1D PC. On the contrary, the reflection coefficient increases about 0.4 at 7.9 THz, and the reflection coefficient decreases about 0.3 at 6.8 THz. Compared with the 1D PC without graphene, the photonic band gap has little change, and the reflection and transmission coefficients are not improved, too. In Fig. 10, for TM_Z wave, the results are the same as TE_Z wave. So, the structure in Fig. 8 cannot improve the optical absorption in THz.

3.3. Graphene in the Bottom of One-Dimensional Graphene Photonic Crystal

Now we consider the case where the graphene is located at the bottom of a spatially periodic array structure of Si/SiO_2. In this structure, we add a spacer of SiO_2 on the surface of 1D PC (seen in Fig. 11).

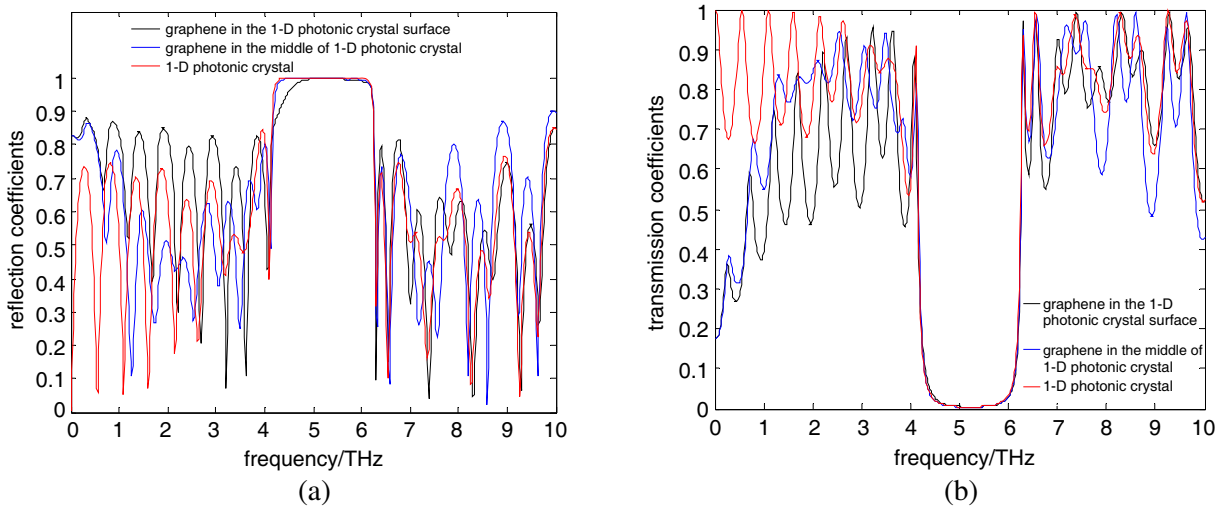

Figure 10. Reflection and transmission coefficients by TM_Z. (a) Reflection coefficients, (b) transmission coefficients.

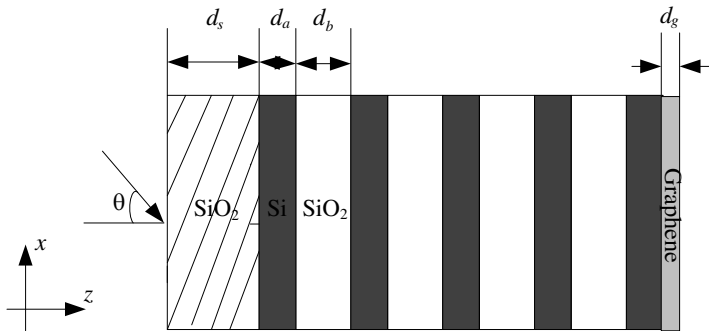

Figure 11. Model of graphene in the bottom of 1-D photonic crystal.

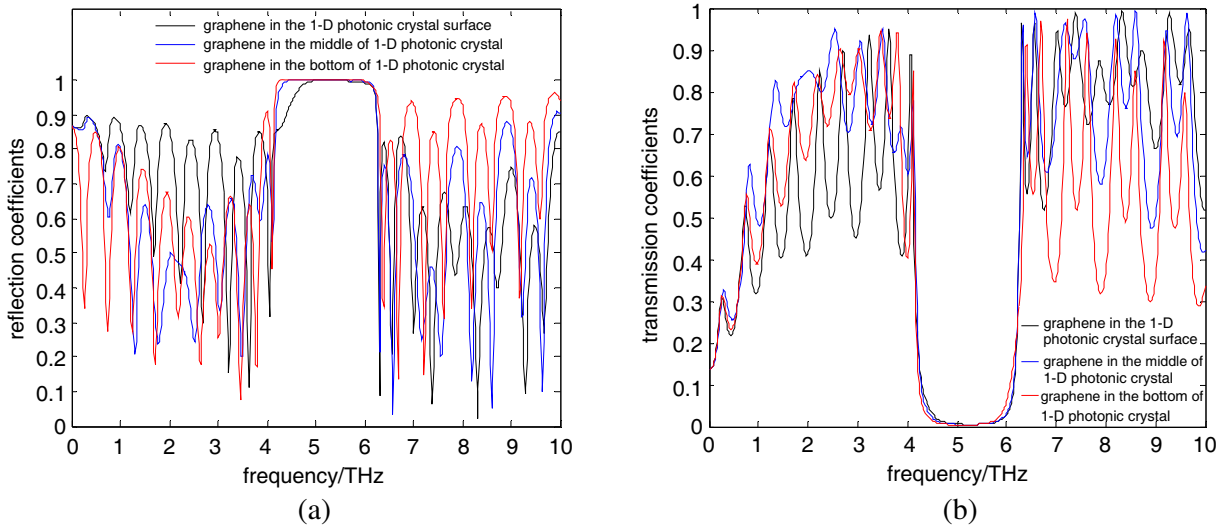

Figure 12. Reflection and transmission coefficients by TE_Z. (a) Reflection coefficients, (b) transmission coefficients.

The reflection and transmission coefficients of this structure by TE_Z and TMz waves for oblique incidence are calculated by the SBC-FDTD method and plotted in Fig. 12 and Fig. 13, respectively. The simulated results show that the photonic band gap is the widest, and the reflection coefficient of the third structure in Fig. 11 is the highest (up to 1.0) among the three structures (Figures 5, 8, 11). The transmission coefficient is less than the other two, and the number of sidelobes of the reflection coefficient increases, but the width and center frequency of the photonic band gap have no change, suggesting that the absorption enhancement cannot be realized by this model, and the characteristics of photonic forbidden band are difficult to be changed. Compared with the results in Fig. 12 and Fig. 13, we can find that the reflection coefficient is the smallest, and the transmission coefficient is the largest when the graphene is located on the surface of 1D PC. So the model of graphene on the surface of GPC is the most ideal.

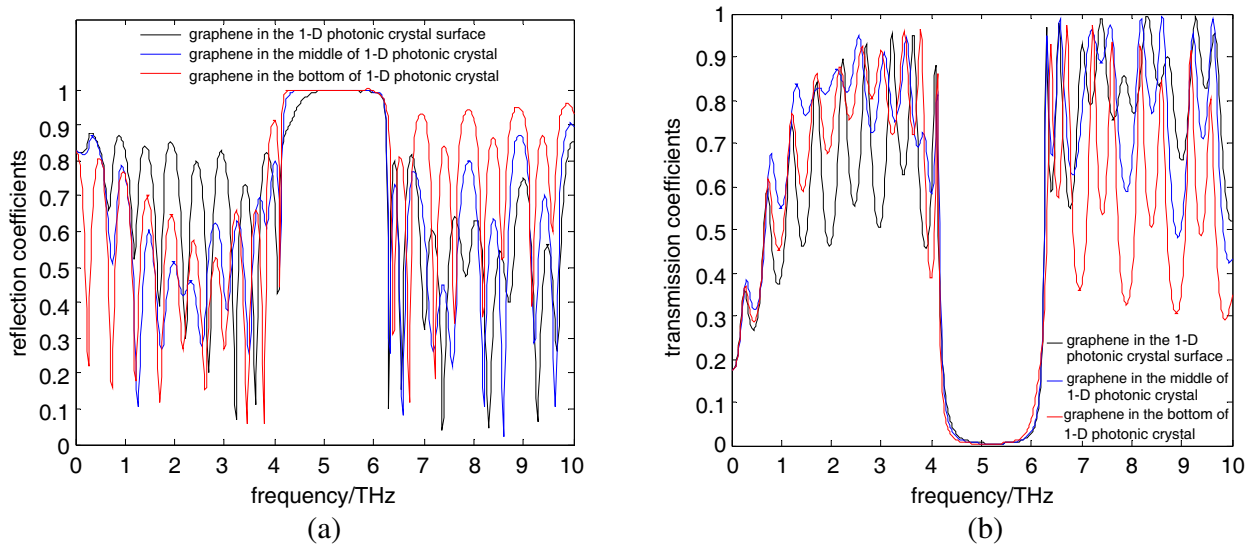

Figure 13. Reflection and transmission coefficients by TM_Z. (a) Reflection coefficients, (b) transmission coefficients.

4. CONCLUSION

In this paper, a 1D SBC-FDTD method is implemented successfully for oblique incidence. The FDTD iterative formulas of the graphene are deduced in the oblique incidence situations for both TEz and TMz waves. The reflection and transmission coefficients of electromagnetic wave by the graphene sheet are calculated in the oblique incidence with $\theta = 30°$. The computed results and analytic solutions are in good agreement. Finally, we study the electromagnetic characteristics of 1D PC with graphene in the oblique incidence situation. By changing the position of graphene in 1D PC, we compute the reflection and transmission coefficients of the 1D PC with graphene in the oblique incidence situation by SBC-FDTD method. The numerical results show that the GPC structure can enhance the optical wave absorption when graphene is located on the surface of 1D PC. These results will provide a theoretical foundation to produce the actual one-dimensional graphene photonic crystal.

ACKNOWLEDGMENT

This work is supported by the National Natural Science Foundation of China under Grant (No. 61072002); Elitist of Liu-Da Summit Project in Jiangsu Province at 2011 under Grant (No. 2011-DZXX-031); and LC acknowledges the support of NSF grant AGS-1405041.

REFERENCES

1. Castro Neto, A. H., R. Guinea, N. M. R. Peres, K. S. Novoselov, and A. K. Geim, "The electronic properties of graphene," *Rev. Modern Phys.*, Vol. 81, No. 1, 109–162, 2009.
2. Moon, J. S. and D. K. Gaskill, "Graphene: Its fundamentals to future applications," *IEEE Trans. Microwave Theory Tech.*, Vol. 59, No. 10, 2702–2708, 2011.
3. Geim, A. K. and K. S. Novoselov, "The rise of graphene," *Nat. Mater.*, Vol. 9, No. 6, 183–191, 2007.
4. Peres, N. M. R. and Y. V. Bludov, "Enhancing the absorption of graphene in the terahertz range," *IOP Science*, Vol. 101, No. 5, 58002, 2013.
5. Liu, J.-T., N.-H. Liu, J. Li, X. J. Li, and J.-H. Huang, "Enhanced absorption of graphene with one-dimensional photonic crystal," *Applied Physics Letters*, Vol. 101, 052104, 2012.
6. Nayyeri, V., M. Soleimani, and O. M. Ramahi, "Modeling graphene in the finite-difference time-domain method using a surface boundary condition," *IEEE Transactions on Antennas and Propagation*, Vol. 61, No. 8, 4176–4182, 2013.
7. Yang, L., Y. Xie, W. Kong, et al., "A novel finite-difference time-domain scheme for electromagnetic scattering by stratified anisotropic plasma under oblique incidence condition," *Acta Physica Sinica*, Vol. 59, No. 9, 6089–6095, 2010.
8. Hanson, G. W., "Dyadic Green's functions and guided surface waves for a surface conductivity model of graphene," *Journal of Applied Physics*, Vol. 103, No. 6, 064302, 2008.
9. Ge, D. and Y. Yan, *Finite-difference Time-domain Method for Electromagnetic Waves*, 3rd Edition, Xi'an University of Electronic Science and Technology Press, Xi'an, 2011.
10. Xie, L., W. Xiao, G. Huang, et al., "Terahertz absorption of graphene enhanced by one-dimensional photonic crystal," *Acta Physica Sinica*, Vol. 63, No. 5, 057803, 2014.
11. Lovat, G., "Equivalent circuit for electromagnetic interaction and transmission through graphene sheets," *IEEE Transactions on Electromagnetic Compatibility*, Vol. 54, No. 1, 101–109, 2012.
12. Gusynin, V. P., S. G. Sharapov, and J. P. Carbotte, "Magneto-optical conductivity in graphene," *J. Phys.: Condens. Matter*, Vol. 19, No. 2, 026222, 2007.